31st Annual International Conference of the IEEE EMBS
Minneapolis, Minnesota, USA, September 2-6, 2009

Intracellular Patterning of Internalized Magnetic Fluorescent Nanoparticles

Peter Tseng, Dino Di Carlo, and Jack W. Judy, *Senior Member, IEEE*

***Abstract*—We have designed, simulated, and fabricated micro-magnetic substrates for the reversible self-assembly of cell-internalized magnetic fluorescent nanoparticles according to lithographically defined patterns within live cells. Magnetic nanoparticles have recently demonstrated potential in activating highly specific activity within single cells. Using microfabrication, we have developed a technique of localizing both particles and large magnetic fields to highly specific, engineered, sub-cellular locations with various modes of operation.**

The substrates were simulated in 3 dimensions with ANSYS FEA, and consist of micro-patterned, electroplated permalloy elements planarized with SU-8. Various modes of magnet-orientation dependent patterns of nanoparticles were generated and verified within live cells, with their precise location verified under separate blue and green (absorption and emission wavelengths of the particles) filters using a fluorescent microscope. Results correspond well with modeled positions and response time. We anticipate using the tool as a compact, simple method of generating highly localized, easily distinguishable, sub-cellular chemical and mechanical signals that is compatible with standard biological fluorescence setups.

I. Introduction and Motivation

MICROSCOPIC and nanoscopic magnetic particles have gained wide acceptance in biological and medical research as a method of selectively controlling biological environments. Traditionally, the particles have been used as a highly specific method of sorting cells, proteins and DNA, and their generation of large fields sensed with detectors to identify quantity, and even detect particle conjugation and size [1-3]. More recently, researchers have conjugated particles with quantum dots for ease of detection, and fabricated porous particles conjugated to enzymes to be used as highly active reaction templates [4-5]. Resonating magnetic beads have been used as remotely activated heat generators [6-7], and in controlling ion channels, mediating signaling, and probing cell mechanics [8-9]. Even with these advances, the potential for this technology and its use on the intracellular level remains largely untapped [4,10], as the modularity of the single cell lends itself to precision studies of highly localized effects.

Micro-Electro-Mechanical Systems (MEMS) technology, and its ability to interface with microenvironments is well suited as a means of interaction with magnetically coupled biological matter. While there has been ample investigation into microfabrication as a means of sorting and manipulation of biological material [11-13], its use in generating magnetically mediated biological activity is scarce. The capability of generating, in a simple fashion, highly localized chemical and mechanical effects could give biologists an unprecedented method of probing cellular architecture, its biochemistry, as well as providing a unique method of generating and studying highly localized cellular signaling.

We have developed a highly compact and simple method of generating and manipulating multiple ensembles of magnetic fluorescent nanoparticles within live cells. This is mediated by a micro-patterned ferromagnetic substrate that is able to generate multiple modes of manipulated patterns. In this study, we report our design and fabrication methods, simulate the achievable magnetic fields with a 3-D ANSYS FEA model while examining the response time of our device, and finally demonstrate the orientation dependent patterning by tracking magnetic fluorescent particle localization in live cells with a fluorescent microscope.

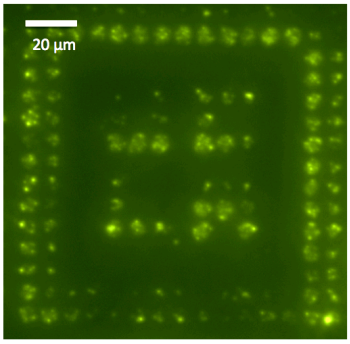

Fig. 1. U C L A spelled out by self-assembled magnetic fluorescent nanoparticles in water (6-µm dots, 3-µm pitch array shown).

II. Magnetic Substrates

A. Design

Our goal for this initial phase of the project is the development of a basic substrate, which along with a simple permanent magnet, can generate large magnetic field gradients and manipulate multiple batches of magnetic nanoparticles at high speed. The generation of large and focused magnetic fields is typically accomplished through a combination of magnetic flux funnels and super fine ferromagnetic tips. Flux funnels, in traditional MEMS processing, are designed as horns for magnetic fields oriented along the plane of the wafer. At this stage we forgo

Manuscript submitted April 7, 2009.

Peter Tseng is with the Department of Electrical Engineering, University of California, Los Angeles, CA 90025 USA (Corresponding author: phone: 310-206-3995; e-mail: ptseng@ucla.edu).

Dino Di Carlo is an Assistant Professor with the Department of Bioengineering, University of California, Los Angeles, CA 90025 USA (e-mail: dicarlo@seas.ucla.edu).

Jack W. Judy is a Professor with the Electrical Engineering Department and the Biomedical Engineering IDP, University of California, Los Angeles, CA 90025 USA (e-mail: jack.judy@ucla.edu).

this typical geometry and instead opt to use large groups of finely patterned ferromagnetic tips, and simple ferromagnetic lines. Micropatterning the ferromagnetic material in this manner focuses the strong magnetic field of the nearby permanent magnetic into locations of high magnetic-field gradient, so that each element acts as a beacon to attract nearby particles. Within a cell, the tiny ferromagnetic islands can generate arbitrary patterns of groups of particles at high speed. As an added benefit, the device displays modal behavior (Fig. 2), as the magnetic potential minima is capable of spanning nearly all *x*-*y* points of the substrate, depending on the orientation of the permanent magnet.

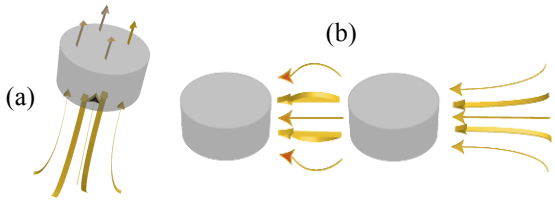

Fig. 2. The two modes of operation for our device: a large permanent field is applied (a) perpendicular to the substrate, and fields are focused through the middle of the dots, and (b) parallel to the substrate, and fields are focused in between the dots.

Our test chip consists of many permutations of ferromagnetic-dot arrays with dots of a diameter of 2 to 6 µm and a pitch of 0.5 to 1 times the dot size. To illustrate the arbitrary-patterning capability of our technology, several demo patterns that spell out letters and words, both with dots and continuous permalloy were included (Fig. 3).

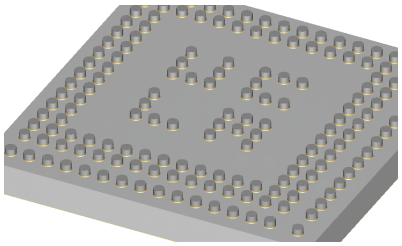

Fig. 3. Solid model of the letters U C L A spelled out in permalloy elements.

B. Simulations

The device performance was modeled by (i) using ANSYS Finite Element Analysis (FEA) to obtain the magnetic field gradients of the elements, and then (ii) using those values to model the response time in MATLAB.

i. Finite-Element-Method Modeling

A 3-D ANSYS Model was used to determine the magnetic field gradients. This was necessary to accurately model the magnetization of the elements, as well as to properly reproduce the effects of the SU-8 planarizing layer that covers the elements. The permeability of the ferromagnetic elements was modeled directly in ANSYS as a hyperbolic tangent function, using the permeability and saturation magnetization of our permalloy. After meshing, nonlinear solutions were obtained for a magnetic flux density of around .6 T. A plot of the magnetic flux density contours at a height 1 µm above the surface of the elements was obtained for two modes of operation is given in Fig. 4.

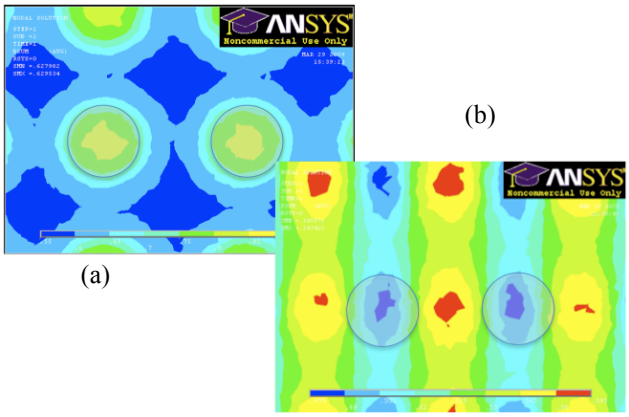

Fig. 4. Plots of magnetic-flux-density contours at a height 1 µm above the surface of the micropatterned element when a magnet is applied from (a) below (contour colors span .55 to .95), and (b) the side (contour colors span .46 to .6). Black outlines the approximate location of the elements.

ii. Response Time

The response time of our devices can be estimated from analyzing the equation of motion for the magnetic nanoparticles, which is given by:

$$m \cdot a_{\text{accel}} = (V_{\text{vol}} \cdot \frac{B_{\text{sat}}}{\mu_o} \cdot \nabla) B - 3 \cdot \pi \cdot \mu_{\text{visc}} \cdot a_{\text{dia}} \cdot v_{\text{vel}} \quad (1)$$

The first term is the magnetic force on a saturated particle (our case), and the second term is the drag force. The gradient of the magnetic flux density is derived from the contours given by ANSYS, and is given in Fig. 5. The rest of the constants are known quantities inherent to the magnetic nanoparticle. For our particle, as given from data sheets, the saturation magnetization is close to 10 mT, and the diameter is 100 nm.

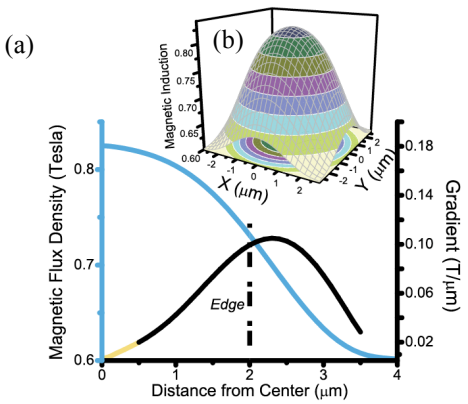

Fig. 5. (a) Plot of the gradient vs. radial distance from center of the element, and (b) curve-fitted contours of magnetic field density around a bottom-excited element.

Eqn 1 is a reasonably complex, coupled partial differential equation. Instead of attempting to solve it directly, we can approximate the solution by chopping our spatial domain

into pieces, and approximating the velocity at each piece with the steady state velocity at that distance:

$$v_{\text{steady state}} = \frac{V_{\text{vol}} \cdot \frac{B_{\text{sat}}}{\mu_o}}{3 \cdot \pi \cdot \mu_{\text{visc}} \cdot a_{\text{diameter}}} \cdot \nabla B(r) \qquad (2)$$

B(r) is given in Fig. 5. This equation remains reasonable at such small scales, where fluidic drag tends to dominate the system. The numerically calculated total time for a particle to be manipulated to the center area (half the diameter of the element) from maximum distance away (directly between the elements) is calculated as 93.6 ms. This value underestimates the response time by a small margin due to the exclusion of cyptoplasm viscosity (a complex function of particle size), and our ignorance of the vertical axis. However this computation remains a reasonable metric for the theoretical time scale at which our device should operate.

C. Fabrication

The magnetic surfaces (Fig. 6) were fabricated on single crystal <100> silicon wafers. The substrates are first cleaned in acetone and Pirahna and then subsequently sputtered with 40 nm of titanium, 250 nm of copper, and 40 nm of titanium. The wafers are then subsequently scored and prepared for photoresist processing. Photoresist (either KMPR 2005 or SU-8 2007) is then spun onto the pieces, and processed to form the electroplating mold for our ferromagnetic elements. Permalloy ($Ni_{80}Fe_{20}$) is then electroplated 3 µm thick onto the wafer. The photoresist is subsequently stripped, and the seed layer etched in three staggered chemical dips of 1% HF (Ti), 5% CH_3COOH / 15% H_2O_2 (Cu), and 1% HF. Next, we deposit a thin layer (200 nm) of low stress nitride at 200 °C, and spin on a 4-µm-thick layer of SU-8, which effectively planarizes the wafer surface. Oxygenating the SU-8 surface with O_2 plasma finishes off the wafer. This final step is typically performed right before the cell tests in order to ensure active surface groups to encourage cell adhesion.

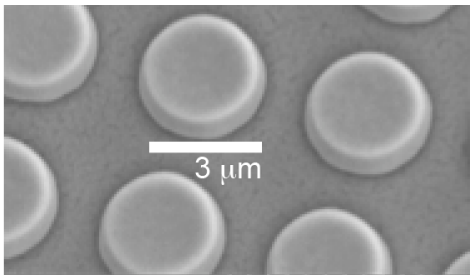

Fig. 6. SEM image of electroplated dots after permalloy mold strip.

III. Experimental Results

A. Magnetic Assembly in Water

Our magnetic fluorescent nanoparticles were purchased from Chemicell (nano-screenMag, dextran, green). For testing, the nanoparticles were diluted in DI water, pipetted into a petri dish, upon which our magnetic surface was inverted for purposes of viewing over an inverted fluorescent microscope. A 1-T rare-earth magnet was used for generating the applied magnetic flux density. Images were taken at set intervals, corresponding with application of and removal of the magnet.

As expected, the bottom-oriented magnet would produce patterns directly above the substrate, as in Fig. 1, and depending on orientation, the potential wells could be tuned to various *x-y* locations above the micropatterned substrate. Since the time required to capture the fluorescent images (5-10 s) was much longer than the response time of the elements, we were unable to precisely quantify the response time. In addition to testing basic patterning capability, we tested for manipulation reversibility (i.e. if the system can return to its original state). As expected from the soft magnetic nature of the components, the system would turn from disperse, to captured, and back to dispersed in 5 min.

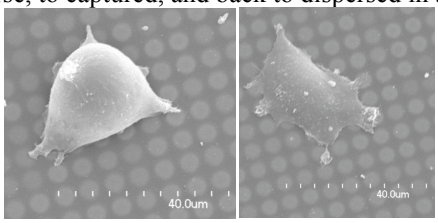

Fig. 7. SEM of fixed cells above planarized substrate.

B. Magnetic Assembly in Living Cells

For our living cell tests, we chose MFC7 breast cancer cells due to their size (25-30 µm across when adhered), and research impact. The cells were grown in Dulbecco's Modified Eagle Media (DMEM), and incubated with the nanoparticles for 48 hr. The cells were then washed multiple times in Phosphate Buffered Saline (PBS), trypsinized, spun down, re-washed, and re-suspended in media. Depending on the run, the cells were simultaneously stained with a diI stain for membrane visualization. Due to the dextran coating and small size of the particles, the continuous washing re-suspends and removes virtually all non-internalized particles from the system. The cells were then placed on the magnetic substrate and left overnight for cell adhesion. The next day the media was washed, and substrate inverted over a PBS-wetted petri dish, so that it could be viewed with a conventional inverted fluorescent microscope.

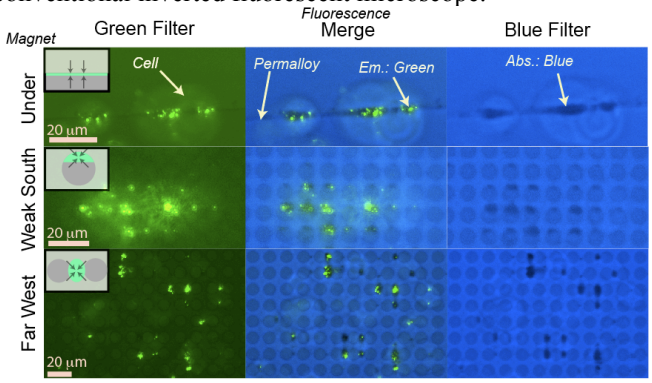

Table 1. Internalized nanoparticle patterns resulting from different magnet orientations and for different structures. Black dots are the most accurate indicator of nanoparticle location.

The various images from Table 1 indicate three disparate signals that are clearly viewable: (1) green-emitting fluorescent particles under the FITC filter, (2) diffuse green auto-fluorescence of the cells, and (3) reflected short wavelengths from the substrate under the DAPI filter that reveals the micropatterned ferromagnetic elements.

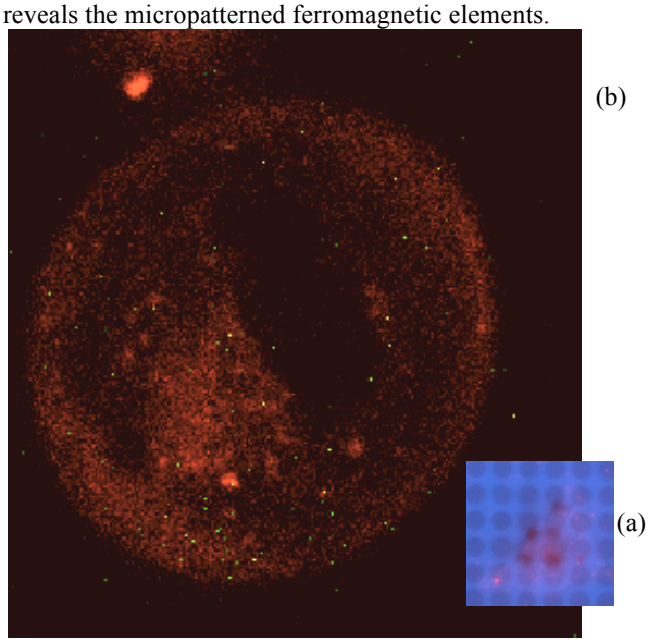

Fig. 8. Membrane stained cell and particles. Note in (a) that the left cell edge strongly disrupts the particle pattern at 2 positions, verifying internal pattern generation. Part (b) is a cross-section at the midpoint of a confocal microscope image. Unfortunately, the weakness of the fluorescent particles yields low signal.

From our experiments, the fluorescence quantum yield of the nanoparticles varies strongly from particle to particle. This is why aligned dark spots on the DAPI filter (bunches of nanoparticles) do not always seem to correspond to a large green emission, or any at all for that matter (Fig. 8). Due to this effect, the most obvious indicator of nanoparticle localization is under the blue DAPI filter, or the absorption band of the particles. Because the absorption contrasts strongly against the light reflected by the array, these images clearly display the manipulated clusters of particles, as well as their orientation to the magnetic elements.

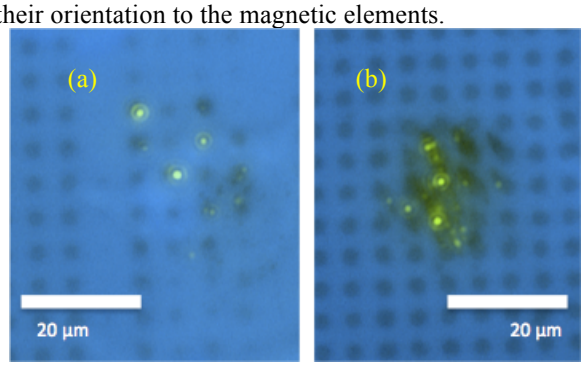

Fig. 9. Known single cells above 3 µm dot / pitch. The fluorescence quantum yield issue is in display here, as in (b), some of the thick pillars of internalized magnetic nanoparticles generate small green fluorescent signal. In the left image, fairly clearly patterned magnetic nanoparticles (darker blacks) generate random signal strengths (requires some careful observation of the FITC filter, green image).

IV. Conclusion

We have demonstrated, to our knowledge, the first generation and manipulation of multiple batches of magnetic nanoparticles within live cells. We anticipate this manner of manipulation as a simple method of generating, and easily locating multiple localized biochemical and mechanical effects within living cells at rapid speeds.

Acknowledgment

We would like to thank the staff of the Nanolab for providing courteous advice in fabricating of our devices, Ira Goldberg for helpful discussions on magnetic particle manipulation, Andrew Fung for microscopy assistance, and Eric Tsang for protocol and materials assistance.

References

[1] L. Guanxiong, et al., "Detection of single micron-sized magnetic bead and magnetic nanoparticles using spin valve sensors," *J. Appl. Phys.,*vol. 93, pp. 7557-7560, May 15 2003.

[2] S. Centi, S. Laschi, M. Franek, and M. Mascini, "A disposable immunomagnetic electrochemical sensor based on functionalized magnetic beads and SPCEs for the detection of PCBs," *Anal Chim Acta,* vol. 538, pp. 205-212, 2005.

[3] M. Stromgberg, J. Goransson, M. Nilsson, and P. Svedlindh, "Sensitive Molecular Diagnostics Using Volume-Amplified Magnetic Nanobeads," vol. 8, no. 3, pp. 816-821, 2008.

[4] J. Gao, W. Zhang, P. Huang, B. Zhang, X. Zhang, B. Xu, "Intracellular Spatial Control of Fluorescent Magnetic Nanoparticles," *J. Amer. Chem. Soc.,* vol. 130, pp. 3710-3711, 2008.

[5] A. Nomura, S. Shin, O.O. Medhi, J.M. Kauffman, "Preparation, characterization, and application of an enzyme-immobilized magnetic microreactor for flow injection analysis," *Anal. Chem,* vol. 76, no. 18, pp. 5498-5502, 2004.

[6] M. Babincova, D. Leszczynska, P. Sourivong, P. Cicmanec, P. Babinec, "Superparamagnetic gel as a novel material for electromagnetically induced hyperthermia," *Journal of Magnetism and Magnetic Mat.,* vol. 225, pp. 109-112, 2001

[7] I. Hilger, R. Hergt, W.A. Kaiser, "Use of magnetic nanoparticle heating in the treatment of breast cancer," *IEEE Proc.-Nanobiotechnology*, vol. 152, no. 1, pp. 33-39, 2005.

[8] J. Dobson, "Remote Control of Cellular Behavior with Magnetic Nanoparticles," *Nature Nano*, vol. 3, no. 3, pp. 139-143, 2008

[9] R. Mannix, S. Kumar, F. Cassiola, M. Montoya-Zavala, E. Feinstein, M. Prentiss, D. E. Ingber, "Nanomagnetic actuation of receptor-mediated signal transduction," *Nature Nano,* vol. 3, pp. 36 – 40, 2007

[10] A. de Vries, B. Krenn, R. Driel, J. Kanger, "Micro Magnetic Tweezers for Nanomanipulation Inside Live Cells," *Biophysical Journal*, vol. 88, pp. 2137-2144.

[11] C. Ahn, M. Allen, W. Trimmer, Y-N Jun, S. Erramilli, "A Fully Integrated Micromachined Magnetic Particle Separator," *J. MEMS,* vol. 5, pp. 151-158, 1996.

[12] J. Do, J-W Choi, C. Ahn, "Low-Cost Magnetic Interdigitated Array on a Plastic Wafer," *IEEE Transactions of Magnetics,* vol. 40, no. 4, pp 3009, 2004.

[13] M. Zborowski, L. Sun, R. Lee, P. Williams, J. Chalmers, "Continuous cell separation using novel magnetic quadrupole sorter," *Journal of Magnetism and Magnetic Materials*, vol. 194, pp. 224-230, 1999.